Journal of Nuclear Materials 377 (2008) 385–395

Contents lists available at ScienceDirect

Journal of Nuclear Materials

journal homepage: www.elsevier.com/locate/jnucmat

# Computer simulation of primary damage creation in displacement cascades in copper. I. Defect creation and cluster statistics

R.E. Voskoboinikov [a,c,*], Yu.N. Osetsky [b], D.J. Bacon [c]

[a] Rolls-Royce UTP, Department of Materials Science and Metallurgy, University of Cambridge, Pembroke Street, Cambridge CB2 3QZ, UK
[b] Computer Sciences and Mathematics Division, Oak Ridge National Laboratory, One Bethel Valley Road, P.O. Box 2008, MS-6138 Oak Ridge, TN 37831, USA
[c] Materials Science and Engineering, Department of Engineering, The University of Liverpool, Liverpool L69 3GH, UK

ARTICLE INFO

*Article history:*
Received 10 April 2007
Accepted 22 January 2008

*PACS:*
61.80.–x

ABSTRACT

Atomic-scale computer simulation has been used to investigate the primary damage created by displacement cascades in copper over a wide range of temperature (100 K $\leqslant T \leqslant$ 900 K) and primary knock-on atom energy (5 keV $\leqslant E_{PKA} \leqslant$ 25 keV). A technique was introduced to improve computational efficiency and at least 20 cascades for each ($E_{PKA}$,$T$) pair were simulated in order to provide statistical reliability of the results. The total of almost 450 simulated cascades is the largest yet reported for this metal. The mean number of surviving point defects per cascade is only 15–20% of the NRT model value. It decreases with increasing $T$ at fixed $E_{PKA}$ and is proportional to $(E_{PKA})^{1.1}$ at fixed $T$. A high proportion (60–80%) of self-interstitial atoms (SIAs) form clusters during the cascade process. The proportion of clustered vacancies is smaller and sensitive to $T$, falling from 30% to 60% for $T \leqslant$ 600 K to less than 20% when $T$ = 900 K. The structure of clusters has been examined in detail. Vacancies cluster predominantly in stacking-fault-tetrahedron-type configurations. SIAs tend to form either glissile dislocation loops with Burgers vector $\boldsymbol{b}$ = 1/2<1 1 0> or sessile faulted Frank loops with $\boldsymbol{b}$ = 1/3<1 1 1>. Despite the fact that cascades at a given $E_{PKA}$ and $T$ exhibit a wide range of defect numbers and clustered fractions, there appears to be a correlation in the formation of vacancy clusters and SIA clusters in the same cascade. The size and spatial aspects of this are analysed in detail in part II [unpublished], where the stability of clusters when another cascade overlaps them is also investigated.



## 1. Introduction

Materials selected for structural components in the core of nuclear power reactors are exposed to a flux of fast neutrons and high temperature. They have to withstand radiation damage processes that occur over wide ranges of time and length, i.e., from defect production at the atomic-level ($\sim 10^{-15}$ s, $10^{-10}$ m) to microstructural evolution over the mesoscale ($\sim 10^{6}$ s, $10^{-3}$ m), without exhibiting a significant degradation of service properties. In order to achieve progress in predictive modelling of property changes across these ranges, atomic-scale computer simulation occupies a special place, for it is able to provide much of the input to models at the higher levels. Large strides in simulating damage production and defect properties have been made over the past decade as a result of the increasing power of computational facilities and in this paper we present results obtained recently for pure copper. Although not actually employed for core structure applications, copper is the archetypal face-centred-cubic (FCC) metal as far as radiation damage is concerned, for it has been studied extensively in order to avoid complications of chemical effects that can occur in austenitic stainless steel, for example, and to exploit its suitability for detailed microscopic examination.

We consider displacement cascades, which are the primary source of radiation damage during fast-neutron irradiation of metals. They are formed by the recoil of primary knock-on atoms (PKAs) with a kinetic energy of more than ~1 keV. The cascade process is characterised by lengths and times of the order of nm and ps, respectively, and cannot be investigated directly by either experimental or analytical techniques. Only atomic-scale computer simulation by the method of molecular dynamics (MD) is suitable for studying the creation of point defects – for reviews see [1–5] and references cited therein – and their stability, mobility and interaction. The latter features are important because point defects cluster directly in the cascade process and the properties of the clusters have important consequences for microstructure evolution and property changes under cascade damage conditions. For example, an imbalance in the proportion of clustered defects of one species versus another, e.g. self-interstitial atoms (SIAs) versus vacancies, creates a complementary

* Corresponding author. Address: Rolls-Royce UTP, Department of Materials Science and Metallurgy, University of Cambridge, Pembroke Street, Cambridge CB2 3QZ, UK. Tel.: +44 1223 33 44 34; fax: +44 1223 33 19 56.
*E-mail address:* rv247@cam.ac.uk (R.E. Voskoboinikov).

0022-3115/$ - see front matter © 2008 Elsevier B.V. All rights reserved.
doi:10.1016/j.jnucmat.2008.01.030

imbalance in the proportion of single defects, which diffuse three-dimensionally and are responsible for solute transport, swelling by void formation and creep, etc. Furthermore, SIA and vacancy clusters formed in close proximity create a weaker stress field than either would individually, and they also facilitate mutual recombination of defects as a result of cascade overlap in high-dose conditions.

A significant fraction of MD studies of cascades was applied to copper (see e.g. [5–15]), treating it as a model FCC metal with low stacking fault energy for fundamental study of radiation damage. However, most studies have treated only a few (typically ≈5) cascades at a given energy and irradiation temperature, and so firm statistics on cluster type and size distribution, particularly as needed for computational models of damage evolution, are lacking. Also, and possibly for the same reason, there appears to be an insufficiency of cluster types observed in earlier cascade simulations, so that it is not easy to compare results of modelling with experimental data. For example, low- and high-temperature experiments on copper have shown efficient production of stacking fault tetrahedra (SFTs) [16–18], but, with the exception of preliminary reports of our work [13–15], SFTs have not been observed systematically in cascade simulation. This is rather surprising because MD simulations of the evolution of a hot, vacancy-rich zone have demonstrated effective formation of SFTs in this environment [19–22]. Thus, we have undertaken an in-depth study of cascades in copper, but to convert MD modelling into a tool that produces not only qualitative information but also reliable quantitative data, it must be verified by a comparison with experimental results. This is not a trivial task because such a comparison can be made only with the predictions of a theoretical model that uses the MD data and the model itself may contain approximations and uncertainties. However, in some cases such comparison can be made with the results of specially designed experiments (e.g. [23–25]) with a reasonable accuracy. This places a requirement on the MD results that they be made realistic by carrying out a large number of cascade simulations and then undertaking detailed analysis of defect structure and properties, and statistical analysis of the results.

For the present work, therefore, we have simulated more cascades (∼450) for a wider range of conditions of irradiation temperature, $T$ = 100–900 K and PKA energy, $E_{PKA}$, = 5–25 keV, and carried out more rigorous structural and statistical analysis than hitherto. The outcome is presented in the following manner. The computational methods used for cascade modelling and analysis are summarised in Section 2. The results for the number of defects created under the different irradiation conditions are presented in Section 3. A significant proportion of both vacancies and SIAs form clusters in the cascade process and statistics for vacancies and interstitials that are not single point defects are presented in Section 4. Typical cluster configurations that arise are described in Section 5. The nature of these is such that only those containing more than a certain number of defects behave as extended defects with at least some characteristics of dislocations, and these are analysed as a function of the irradiation conditions in Section 6. The results are discussed and conclusions drawn in Section 7.

We have computed the size distribution of the population of defect clusters in the MD modelling and compared the vacancy data with experiments on neutron-irradiated copper [24]. These results are to be reported in another paper, referred to here as part II [26]. The simulations indicate a correlation in the size and spatial arrangement of vacancy and SIA clusters formed in the cascade process, and this is also assessed in part II. Finally, we have investigated stability of typical SIA and vacancy clusters in copper against overlap by later displacement cascades, a situation that is common in neutron-irradiated copper when SFTs produced with high number density (up to $\sim 10^{24}$ m$^{-3}$) may overlap with new cascades. This part of the study is also presented in part II.

## 2. Simulation technique

### 2.1. MD method

An equilibrium, short-range, many-body interatomic potential [27] was used for the simulations. With this potential, the point defect formation energy for a vacancy and <100> dumbbell SIA is 1.19 eV and 3.62 eV, respectively. The vacancy migration energy is 0.69 eV. The melting point is ≈1250 K [22,28] and the energy of the intrinsic stacking fault on a {111} plane is estimated as 20–36 mJ m$^{-2}$ [22,27–29]. Although newer interatomic potentials for copper exist [30] they reproduce nearly the same behaviour. The close similarity of the potentials is obvious from the comparison of calculated lattice properties, defect energies and values of planar fault energies, see [27] and [30] for further particulars. However, in contrast to the embedded atom type potentials [30] with non-analytical embedded function the Finnis–Sinclair type one [27] is computationally cheaper because of simple analytical form of the embedded function. The pair part of the potential used was modified for small interatomic separation by fitting to the Universal Screened Coulomb repulsion function for Cu–Cu interactions [31].

Four ambient crystal temperatures were considered, namely 100, 300, 600 and 900 K. A low temperature (such as 100 K) was used for most previous computer simulation studies, whereas the higher temperature range is more consistent with conditions met by metals in practical situations. The model crystals were equilibrated for about 50 ps prior to initiation of the PKA. The MD simulation box had cubic shape with {100} faces. It was maintained at constant volume, with lattice parameter $a_0$ set to the zero-pressure value for the chosen temperature (see Table 2 of Ref. [15]). Periodic boundary conditions with no energy/temperature damping were employed. The number of atoms in the box was chosen in accordance with the values of $E_{PKA}$ and $T$, and is given in Table 1. The MD box size was larger than those used previously for a similar $E_{PKA}$ and $T$ condition, thereby leading to a smaller increase in lattice temperature once the PKA energy was dissipated. (The temperature increase did not exceed 80 K in any of the simulations.)

From 20 to 50 cascades for each PKA energy and ambient temperature were simulated in order to ensure statistical reliability of the results and obtain as many point defect clusters of various configurations, shapes and sizes as possible. The actual number of cascades is recorded in Table 1. PKAs were introduced along high-index crystallographic directions such as <123>, <234>, <345>, <135> and <112> in order to avoid recoil-atom channelling events, which are quite possible especially at low $T$ and high $E_{PKA}$. (To study channelling by MD it would be necessary to use boxes with unreasonably large numbers of atoms. However, a channelled atom experiences a low rate of energy loss until it is defocused and so channelling would not have a significant effect on the data reported here. This would not be the case at higher energy where sub-cascade formation becomes dominant.) PKAs were created at different sites in the box at different times so that (quasi-)random spatial and temporal PKA distributions were simulated. The centre of the simulation box was repeatedly shifted to the centre of gravity of kinetic energy of the constituent atoms. Furthermore, the likelihood of a cascade extending beyond the box boundary and re-entering via periodic conditions was minimised. This is reflected in the small number of simulations abandoned in this research: only seven events in more than 450 simulations had to be stopped due to adverse channelling. It also lessened the selectivity effect in which there is a tendency for

**Table 1**
Number of atoms in the MD simulation box and number of cascades simulated for the different combinations of temperature and PKA energy considered

| $T$ (K) | 5 keV | | 10 keV | | 15 keV | | 20 keV | | 25 keV | |
|---|---|---|---|---|---|---|---|---|---|---|
| | Atoms | Cascades | Atoms | Cascades | Atoms | Cascades | Atoms | Cascades | Atoms | Cascades |
| 100 | 500 000 | 20 | 500 000 | 20 | 500 000 | 25 | 2 048 000 | 20 | 2 048 000 | 52 |
| 300 | 296 352 | 20 | 500 000 | 20 | 500 000 | 20 | 1 048 576 | 20 | 2 048 000 | 20 |
| 600 | 296 352 | 20 | 500 000 | 20 | 500 000 | 20 | 1 048 576 | 20 | 1 048 576 | 19 |
| 900 | 296 352 | 20 | 500 000 | 20 | 500 000<br>1 048 576 | 20<br>10 | 1 048 576 | 20 | 1 048 576 | 20 |

debris from the more compact cascades to be over-represented in the final statistics.

### 2.2. Modelling the cascade ballistic phase

At a time in the early stage of a cascade, a small proportion of atoms recoil with high velocity while the rest satisfy the equilibrium velocity distribution for the ambient temperature. However, convergence of the MD algorithm for integrating the equations of motion of the atoms is governed by the time-step, $t_s$, of the fastest atom, and the time-step for a PKA with energy $E_{PKA} = 20$ keV is many orders of magnitude lower than that for atoms equilibrated at, say, $T = 100$ K. Use of small $t_s$ over all atoms in the initial stage of a cascade is computationally inefficient, and in order to accelerate calculations in this stage a variable time step algorithm [32] was implemented, as follows.

The ensemble of atoms is divided into subsets 'hot' and 'cold'. The former consists of atoms with velocity $v$ in the range $pv_{max}$ to $v_{max}$, where $v_{max}$ is the velocity of the fastest atom at that time, and atoms in layers of thickness $d_{hot}$ surrounding these fast atoms. The latter comprises the rest. This designation allows separate integration of two micro-canonical ensembles that have essentially different parameters (temperature distribution and time-step). Time-step $t_s$ is determined by the condition that the fastest atom does not travel by more than $qa_0$ in one step. Integration of the equation of motion of atoms in the hot region(s) is applied with $t_s$ calculated repeatedly in this way for $n_{hot}$ steps while the cold atoms remain stationary. The total time, $t_{cold}$, of the $n_{hot}$ steps is calculated, following which the cold atoms are moved with time-step $t_{cold}$ and their new velocities obtained. The velocity distribution in the system is then analyzed, new hot and cold volumes are determined and separate integration is repeated for the two subsets. The shape of the hot region(s) depends on the PKA energy and the stage of cascade evolution. It is rather irregular at the beginning, especially for high PKA energy when processes such as channelling and sub-cascade initiation occur. As the primary and higher-order knock-on atoms exchange kinetic energy with cold matrix atoms, the hot volume grows and eventually the distinction between hot and cold disappears. When the whole simulated volume is assigned as hot, the equations of motion of all atoms are integrated with the same time-step. The velocity-Verlet algorithm [33] was applied for integration throughout.

The parameter set for this technique was chosen from trial simulations to test for total energy conservation. The settings were as follows $p = 1/30$, $q = 0.007$, $n_{hot} = 10$ and $d_{hot} = 2.5a_0$, which is the effective range of the interatomic potential. This choice errs on the conservative side and defines the two ensembles of hot and cold atoms such that they stay in thermodynamic equilibrium with each other. Both ensembles are micro-canonical and total energy conservation within the usual fluctuations is therefore automatically fulfilled. There cannot be direct coincidence of damage caused by displacement cascades evaluated using accelerated and conventional techniques because no two cascades are exactly the same, even with the same simulation method. However, the conditions for energy conservation with the same interatomic potential ensure that the spectra of total number and clusters of defects are equivalent (within the statistical variations) for the two techniques.

Fig. 1 provides an example of the evolution of the time-step (broken line), average temperature (black solid line) over the MD cell and number of atoms displaced from their lattice sites (thick grey line) on the number of integration steps for a 20 keV cascade in a crystal at $T = 100$K. The time-step was relatively large (~4 fs) during initial equilibration of the crystal at 100 K, but then decreased by more than three orders of magnitude (to ~0.001 fs) when the PKA was introduced. It increased gradually in the ballistic phase as $E_{PKA}$ was distributed by collisions among more and more atoms, and then faster as more kinetic energy was converted to potential energy by displacement of these atoms. After the number of displaced atoms, and thus the potential energy, reached a maximum, most atoms returned to lattice sites, resulting in release of the potential energy and corresponding increase in $T$. The time-step increased slowly in this thermal-spike phase until the whole crystal became 'hot' and $T$ stabilised at the final value of 142 K. At this point (~20–30 ps) a uniform time-step of about 4 fs was applied. The MD routine was stopped when the number of point defects remained constant for 50 ps ($T = 100$ K, 300 K) or 30 ps ($T = 600$ K, 900 K). In some cases, short-term evolution of damage was studied by continuing the simulation to 150 ns or more.

### 2.3. Defect and cluster analysis

Unambiguous identification of point defects and their clusters is challenging when a large number of cascades has to be treated. Three different methods were applied here. One is based on analysis of Wigner–Seitz (WS) cells and is used to identify vacant sites (=cells with no atoms) and SIAs (=cells with more than one atom).

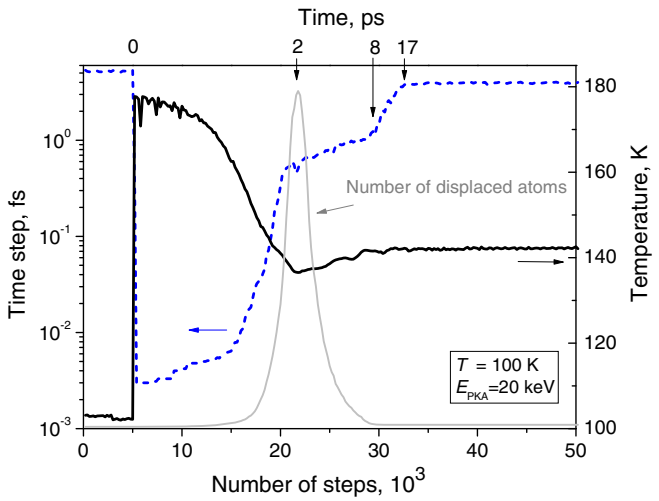


**Fig. 1.** Variation of MD time-step, $t_s$, and crystal temperature (obtained from average kinetic energy of the atoms) with number of time steps for a 20 keV cascade in a model initially at 100 K. The number of displaced atoms obtained by the ES analysis is superimposed.

This method is adequate[1] for determination of the number of surviving vacancies and SIAs, but is not appropriate for identification of structures with correlated atomic displacements typical of stacking faults and interstitial dislocation loops with perfect Burgers vector. The second is equivalent spheres (ES) analysis – sometimes called displaced-atom analysis – based on the position of atoms with respect to lattice sites. For each lattice site the closest distance to an atom is evaluated, and if larger than a threshold value the site is treated as vacant. Contrariwise, for each atom the closest distance to a lattice site is determined, and if larger than the threshold value the atom is treated as 'displaced'. The threshold displacement used here was $0.27a_0$. Evaluation of the number of point defects is not straightforward in this approach. The third method, cluster configuration analysis, uses the output of ES analysis to identify a point defect cluster in the following manner. Since the highest value of the di-vacancy binding energy in copper occurs when the two vacancies are in first-nearest-neighbour coordination, and similarly for the two SIAs in a di-interstitial configuration, we assume that, irrespective of its type, a point defect belongs to a cluster provided there is another point defect belonging to the cluster in the first coordination sphere. Cluster type is defined by the imbalance between constituent vacant sites and displaced atoms assigned to the cluster. The overall number, $N_{FP}$, of surviving Frenkel pairs is the sum of vacancies (not vacant sites) over all single vacancies and vacancy clusters, $N_v$, which equals the sum of SIAs (not displaced atoms) over all single SIAs and SIA clusters, $N_i$. (Conservation of atom number was assured by checking that $N_v = N_i$.)

## 3. Number of Frenkel pairs

The variation of $N_{FP}$, with $E_{PKA}$ four all four temperatures is shown in Fig. 2, where each point is the result from one cascade. The Figure emphasizes the dispersion of the $N_{FP}$ values for a given condition, particularly at high energy and temperature, and points to the importance of our intention to obtain reliable and statistically comprehensive values for the population of point defects by conducting a large number of simulations for each $E_{PKA}$ and $T$ combination.

The mean value of $N_{FP}$ for all 20 irradiation conditions is shown in Fig. 3(a). Standard deviation is shown by bars. The dependence on PKA energy exhibits clear behaviour in which both $N_{FP}$ and its dispersion increase with increasing $E_{PKA}$ at all temperatures. There is no significant change in $N_{FP}$ as $T$ increases from 100 to 300 K, but it falls markedly as $T$ increases to 600 K and then to 900 K in the higher part of the energy range. There is no $T$-dependence in $N_{FP}$ at 5 keV. The Norgett, Robinson and Torrens (NRT) model [34], which is based on binary collision treatment and uses an average threshold displacement energy of 30 eV [35], gives much higher numbers than the mean $N_{FP}$ values shown in Fig. 3(a), i.e. 67 for $E_{PKA} = 5$ keV and 333 for $E_{PKA} = 25$ keV. The MD values are only 16% of the NRT number for all temperatures at 5 keV, and between 14% and 20% of that number at $E_{PKA} = 25$ keV.

The data are plotted on logarithmic scales in Fig. 3(b) in order to test the validity of the power-law formulation $N_{FP} = A(E_{PKA})^m$, which was found in [2] to give a good fit to data from MD simulations for cascades with $E_{PKA} \leqslant 10$ keV when $m \approx 0.75$. (The number predicted by the NRT formula has $m = 1$ and is also shown in Fig. 3) The best-fit lines through data from the present work have values of $m = 1.10 \pm 0.05$ and $A = 1.7 \pm 0.1$ (with $E_{PKA}$ in keV), where the ± limits correspond to $T = 100$ K and 900 K, respectively. Interestingly, Stoller [36] reported that $m$ is 0.8 for cascades with $E_{PKA}$ less than about 20 keV in iron at 100 K and 1.12 for higher energy. The

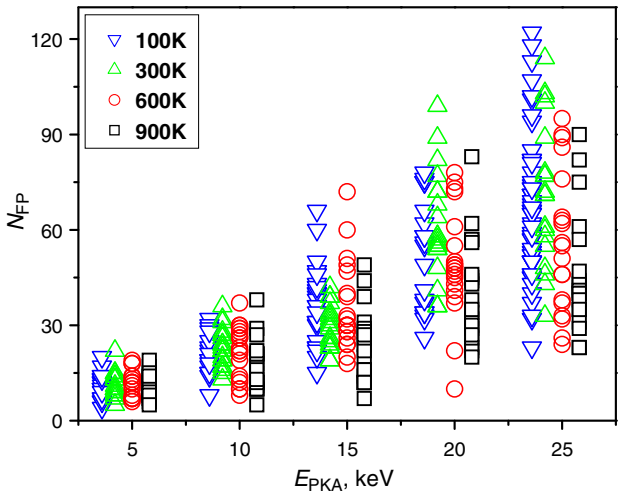


**Fig. 2.** Number of Frenkel pairs vs. PKA energy for the four irradiation temperatures. Each point is the result from one cascade and the data are displaced slightly from their actual $E_{PKA}$ values to assist clarity.

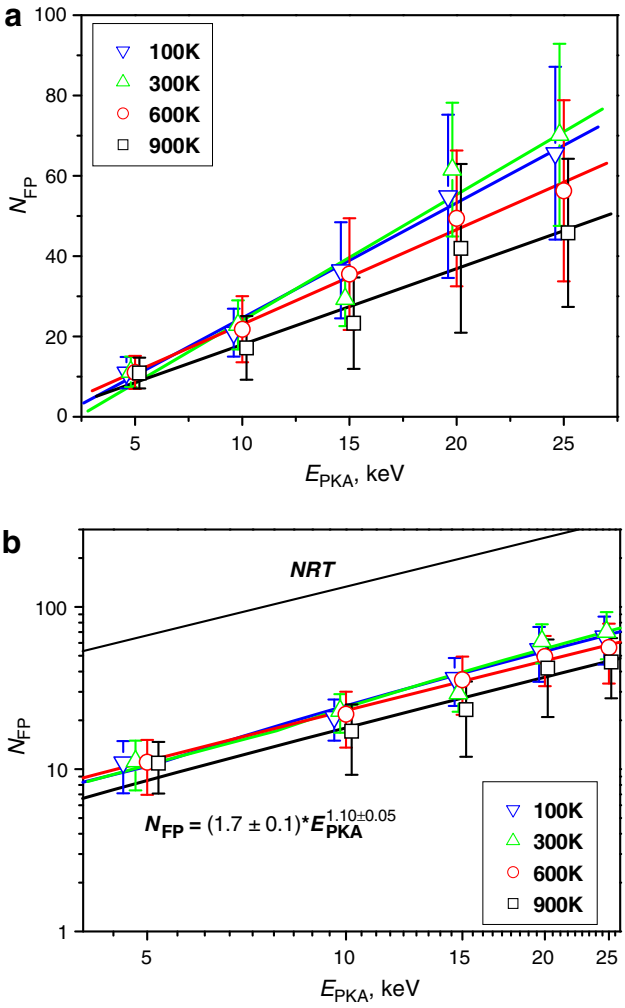


**Fig. 3.** (a) Mean value of the number of Frenkel pairs plotted in Fig. 2. Bars show the standard deviation. (b) The same data redrawn with logarithmic scales. Comparison with the NRT prediction is provided. The four best-fit lines $N_{FP} = A(E_{PKA})^m$ drawn through the means have the range of $A$ and $m$ values indicated.

[1] In certain cases, particularly at elevated temperatures in strained regions when three atoms are in the same cell, Wigner-Seitz cell analysis can produce an incorrect number of Frenkel pairs.

higher value was believed to be due to the onset of sub-cascade formation at high $E_{PKA}$. We ascribe the higher exponent in copper at low PKA energies to higher stability of SIA and vacancy clusters in that metal, see Fig.7(a) and (b), which prevents recombination. The relevant cluster formation issues are discussed in detail in part II of this report.

There are several possible explanations for the contrast between the decrease of $N_{FP}$ with increasing $T$ at high PKA energy and its insensitivity to $T$ at low energy. First, an increase in ambient temperature slows down heat transfer from the cascade region to the periphery of the simulation box. The corresponding increase in thermal spike lifetime raises the probability of recombination of point defects. Second, high-amplitude thermal oscillations of atoms at high temperature prevent channelling events for recoiling atoms. This effect results in more-localized cascades with shorter distances between neighbouring defects, and so facilitates mutual recombination as well. Third, clustering of point defects, particularly SIAs, restricts the dimensionality of their motion and thereby lessens their loss by recombination: as will be seen, formation of clusters of point defects and cluster stability depend on temperature. We now consider direct formation of vacancy and SIA clusters in displacement cascades in copper.

## 4. Clustered fraction of defects

The fraction of vacancies in a cluster with at least one other nearest-neighbour vacancy at the end of the thermal spike phase varies widely from 0% to about 90% for the conditions studied here. This is shown in Fig. 4(a), where the fraction, $\varepsilon_2^v$, of vacancies in clusters of two or more is plotted as a function of $E_{PKA}$ for all cascades. Despite the wide dispersion in the data, trends can be discerned, as seen in Fig. 4(b), where the mean value of $\varepsilon_2^v$ and the standard deviation are plotted for all 20 conditions. For the range 100–600 K, the mean clustered fraction increases from about 30 to 40–60% as $E_{PKA}$ increases from 5 to 25 keV, with no significant $T$-dependence. When $T$ is increased further to 900 K, however, $\varepsilon_2^v$ still increases with $E_{PKA}$ but it is approximately halved in value. Since the total number of vacancies at this temperature is also small (Fig. 3), the population of clustered vacancies is very much smaller at 900 K.

Similar plots for the SIAs are presented in Fig. 4(c) and (d). The dispersion in the data for each $E_{PKA}$ and $T$ combination is not as wide as found for the vacancies, except at low energy, and the dependence of $\varepsilon_2^i$ on $E_{PKA}$ is clearer. Between 40% and 90% of the SIAs are formed in clusters during the cascade process, with little dependence on temperature.

## 5. Typical configurations of cascade debris and defect clusters

The large variety in cascade form and defect structure found for every condition of $E_{PKA}$ and $T$ requires description before proceeding with further analysis. Cascades at one extreme have their defects widely dispersed in the crystal: these defects tend not to form large clusters in the cascade process. Other cascades can be

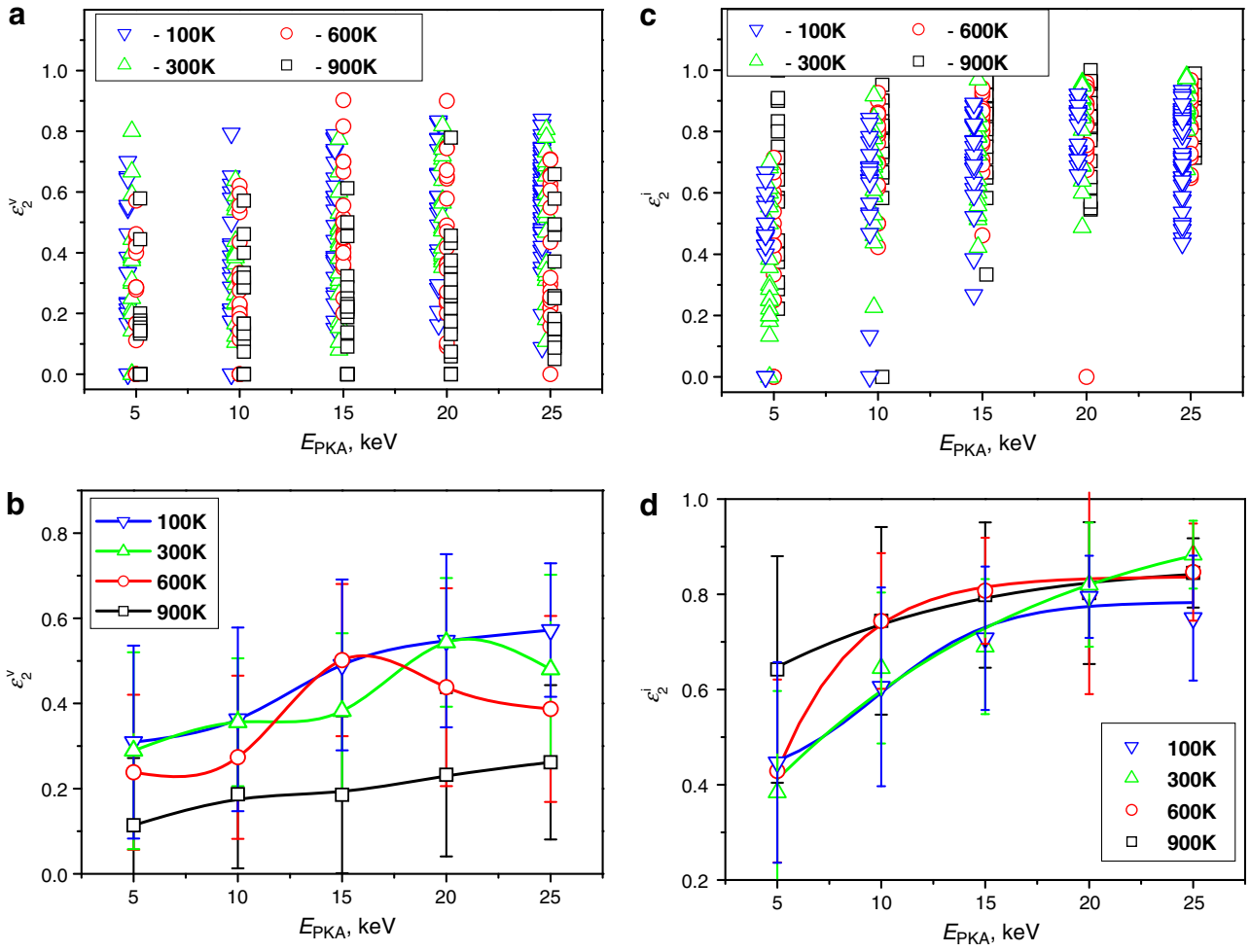


**Fig. 4.** Fraction, $\varepsilon$, of defects in clusters of size two or more: (a) vacancy data for individual cascades; (b) mean values with standard deviation for vacancies; (c) SIA data for individual cascades; (c) mean values with standard deviation for SIAs.

quite localised and tend to create larger clusters. An example of each is shown in Fig. 5(a) and (b). These visualisations based on ES analysis of debris in two 25 keV cascades show vacant sites and displaced atoms as dark and light spheres (red and cyan in colour version), respectively. $N_{FP}$ was 60 and 206 for the cascades in (a) and (b), respectively. Most of the defects in the latter are either in the central polyhedral cluster with {1 1 1} faces containing 181 vacancies or the interstitial cluster with 195 SIAs at the upper right. Thus, cascade form rarely follows the conventional picture of a vacancy-rich core surrounded by a mantle of interstitials.

In view of the variety of defects observed, we have identified the typical configurations into which most clustered arrangements fall. Their visualisations by ES analysis are presented in Fig. 6 and are as follows. Vacancy clusters are shown in (a)–(c). The cluster in Fig. 6(a) is an almost regular SFT, with intrinsic stacking fault on its four {1 1 1} faces and stair-rod partial dislocations along its six edges. The cluster in Fig. 6(b) is an example of two conjoined SFTs. The three-dimensional vacancy cluster shown in Fig. 6(c) has {1 1 1} faces like an SFT, but cannot be identified as a regular polyhedron. Interstitial clusters mainly have one of two forms. Frank loops with Burgers vector $\boldsymbol{b} = 1/3\langle 1\,1\,1\rangle$ enclosing an extrinsic stacking fault are visualised as a platelet of SIAs on a {1 1 1} plane. Two are seen on either side of an SFT-like vacancy cluster in Fig. 6(d). Most of the remaining interstitial clusters are small dislocation loops with the perfect $\boldsymbol{b} = 1/2\langle 1\,1\,0\rangle$. They consist of sets of parallel <1 1 0> crowdions

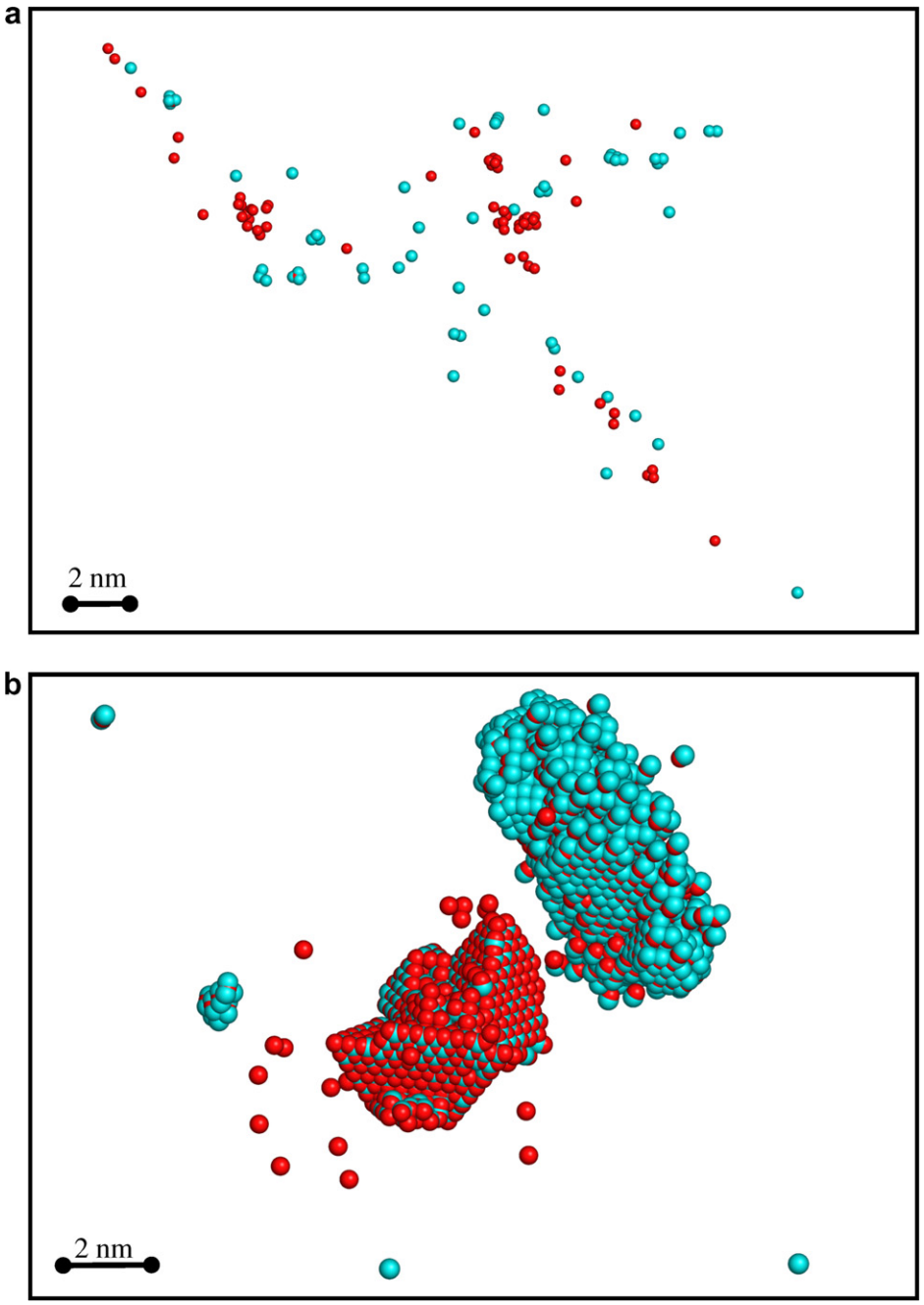


**Fig. 5.** Computer-generated visualisations of damage created in 25 keV cascades at 100 K where the defects are either (a) well-dispersed or (b) localised. Vacant sites and displaced atoms are shown as dark and light grey spheres (red and cyan in colour versions), respectively.

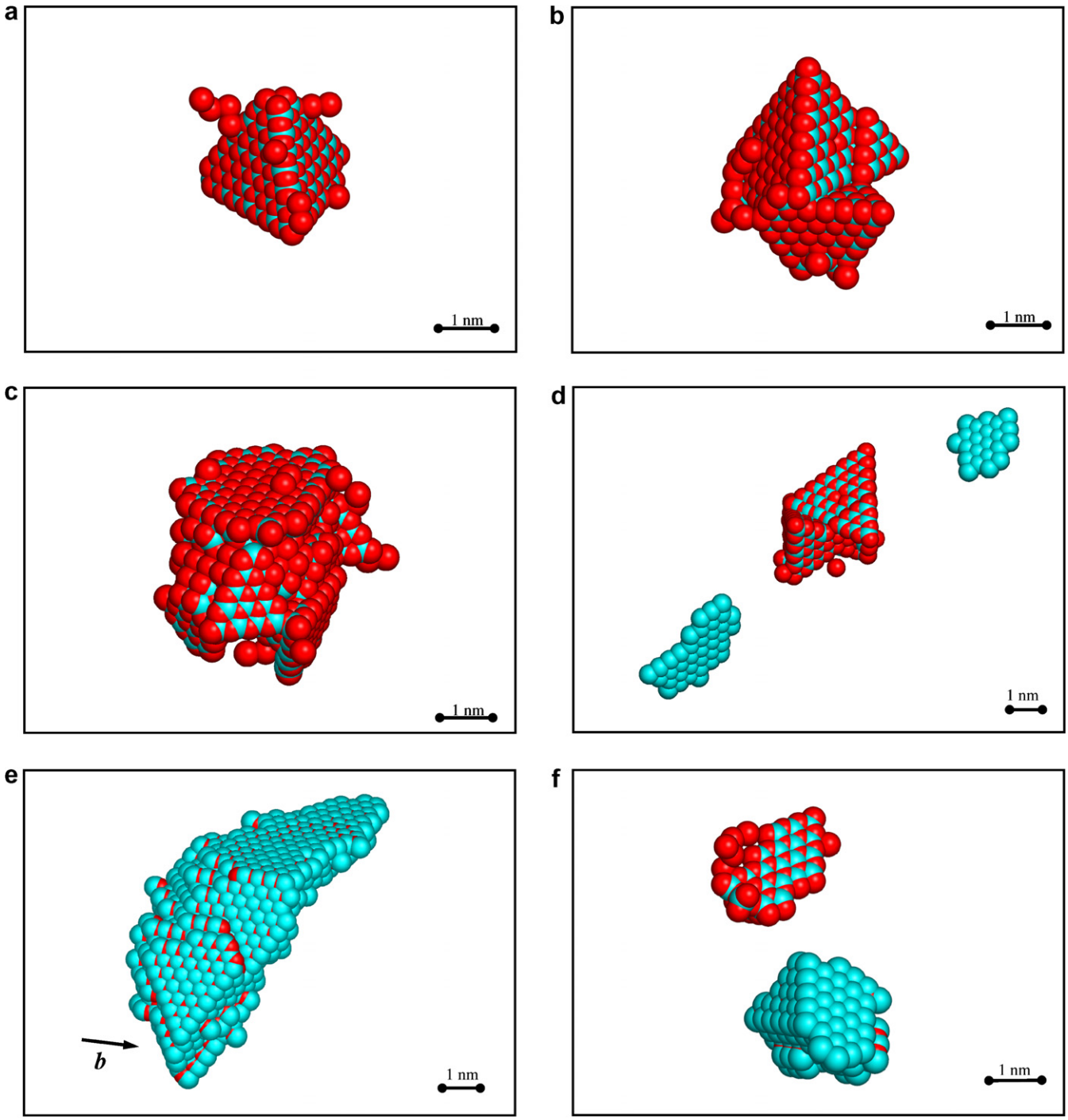


**Fig. 6.** Typical SIA and vacancy clusters found in displacement cascades. (a) Nearly regular SFT formed by 42 vacancies. (b) Two conjoined SFTs (92 vacancies). (c) Irregular SFT-like vacancy cluster (209 vacancies). (d) Two sessile Frank loops (37 and 22 SIAs) in the vicinity of an SFT-like vacancy cluster (91 vacancies). (e) Glissile SIA dislocation loop of 146 SIAs. (f) Sessile 3-D 46 SIAs cluster with {1 1 1} faces (below) and small SFT-like vacancy cluster of 33 vacancies (above).

and are seen as rows of displaced atoms and vacant sites in the ES visualisations. They are observed to be mobile in the direction of $\boldsymbol{b}$ in the timescale of a simulation. An example of a large glissile cluster is provided in Fig. 6(e), where an arrow indicating $\boldsymbol{b}$ is added for clarity. Sessile SIA clusters with irregular 3-D configuration and low-index facets were also formed occasionally – Fig. 6(f) contains an example – but annealing simulations on other defects of this type show that they transform to the more stable arrangement with $\boldsymbol{b} = 1/2\langle 1\,1\,0\rangle$ during further post-cascade annealing.

## 6. Clusters with extended defect character

### 6.1. Clustered fraction

Clusters containing only a few vacancies or SIAs have some characteristics that are similar to those of single point defects. For example, their atomic configuration is simply the superposition of the structure of the individual vacancies or interstitials and, like the singles of the species, they are able to migrate three-dimensionally [37]. Larger clusters tend to adopt different

configurations from these, however, and behave differently in response to stress and temperature. MD studies of motion of SIA clusters in copper have shown that those of size of four or more migrate one-dimensionally along a <110> crystallographic axis without changing direction during the timescale (~tens of ns) of MD simulation [37]. This restricted behaviour of the larger clusters is significant for evolution of radiation damage [38] and, as discussed in Section 5, they become perfect interstitial dislocation loops with $\boldsymbol{b} = \frac{1}{2}\langle 110\rangle$ as they become larger. Copper is an FCC metal with low stacking fault energy, and it was seen in Section 5 (Fig. 6(d)) that a population of sessile faulted (Frank) dislocation loops is also formed in cascades. They, too, should convert to perfect loops during growth by subsequent absorption of more SIAs. Larger groups of vacancies, on the other hand, collapse to form immobile SFT-like structures (see Fig. 6(a)–(c)). The minimum number of vacancies for this to occur is three, for relaxation of atoms around a tri-vacancy of nearest-neighbours results in four vacancies at the vertices of an elementary tetrahedron with edge of size $a_0/\sqrt{2}$ and one atom displaced to the centre of the tetrahedral hole.

Thus, in order to exclude clusters that have point-defect character rather than extended-defect, dislocation character, we now reanalyse the data so that the smallest size considered is three or more for vacancy clusters and four or more for interstitial clusters.

The dependence of the mean value, $\varepsilon_3^v$, of the fraction of clusters containing three or more vacancies on $E_{PKA}$ and $T$ is shown in Fig. 7(a). Again, the spread of values among cascades for the same $E_{PKA}$ and $T$ is large (from 0% to 80%). In general terms, three energy ranges are apparent: $E_{PKA} \leqslant 10$ keV, $E_{PKA} \geqslant 15$ keV and the transition between. The fraction of vacancies in SFT-like clusters does not exceed 20% at low PKA energy ($\leqslant$10 keV) or at any energy at $T = 900$ K. Approximately 30% to 50% of all vacancies produced by PKAs with energy $E_{PKA} \geqslant 15$ keV are formed in clusters at low temperatures ($\leqslant$600 K). $\varepsilon_3^v$ is small and exhibits weak dependence on PKA energy at 900 K.

The mean value, $\varepsilon_4^i$, of the fraction of SIAs in clusters containing four or more defects is shown in Fig. 7(b). The range of individual cascade values for any energy is wide (from 0% to 100%). The fraction is low (approximately 20%) at 5 keV and low $T$, but increases with increasing energy to the range 60–80% at higher PKA energy. Overall, the maximum of fraction $\varepsilon_4^i$ is larger than that of $\varepsilon_3^v$, viz. 80% compared with 50% at high energy, and increases rather than decreases with increasing $T$.

### 6.2. Cluster size and yield

The mean size (number of vacancies) in the clusters reported in Fig. 7(a) is plotted as a function of temperature and cascade energy

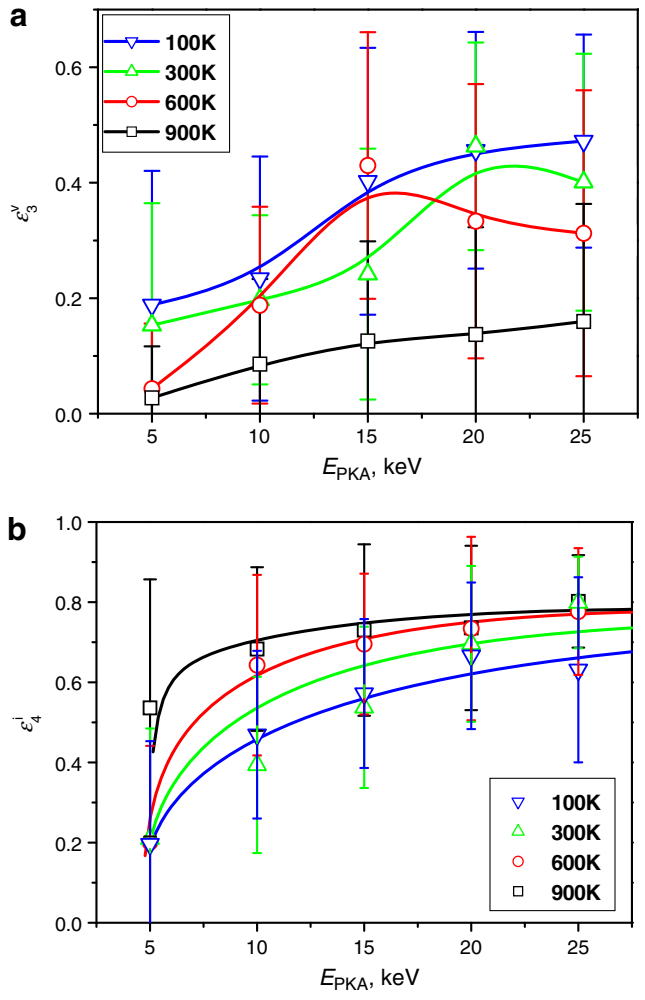


**Fig. 7.** Mean values of the fraction, $\varepsilon$, and standard deviation, of (a) vacancies in clusters containing three or more defects and (b) SIAs in clusters containing four or more defects.

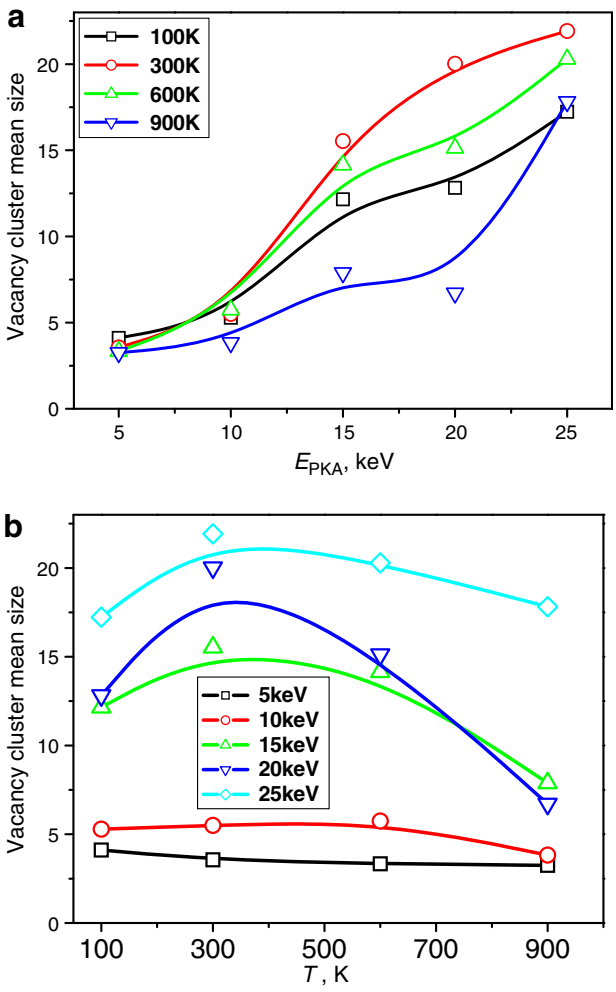


**Fig. 8.** Variation of the mean number of vacancies per vacancy cluster versus (a) cascade energy and (b) irradiation temperature. The means are the average over all clusters of size three or more.

in Fig. 8(a) and (b), respectively. (Note that this is the mean size averaged over clusters, not per cascade.) Fig. 8(a) reveals a marked transition in mean size between the low-energy ($\leqslant$10 keV) and high-energy ($\geqslant$15 keV) regimes. The former gives rise to a mean size of 3–6 vacancies, independent of $T$, whereas the latter results in the largest mean size of 15–22 vacancies at 300 K and a marked decline in size as temperature rises to 900 K. The mean number of vacancy clusters of size three or more created per cascade ('cluster yield') is plotted against $T$ and $E_{PKA}$ in Fig. 9(a) and (b), respectively. Here the trends are clear. The yield not only decreases with decreasing cascade energy, it also decreases with increasing crystal temperature.

Similar data for the SIA clusters with four or more defects are plotted in Fig. 10(a) and (b) for size and yield per cascade, respectively. The mean number of SIAs per cluster plotted against $T$ in Fig. 10(a) exhibits strong transition from low to high energy between 10 and 15 keV, as in the vacancy data. However, unlike the vacancy clusters, the mean size of the interstitial clusters continually increases with increasing $T$.

The effects seen in these figures can be explained quantitatively as follows. As temperature increases from 100 to 300 K, cascades tend to have a more compact form, mainly due to increasing amplitude of thermal oscillations of atoms giving rise to stronger defocusing of primary and higher-order recoils. The more compact cascade core results in a higher yield and larger size of vacancy clusters. As temperature increases further, however, the combination of high $T$ and increased lifetime of the thermal spike not only

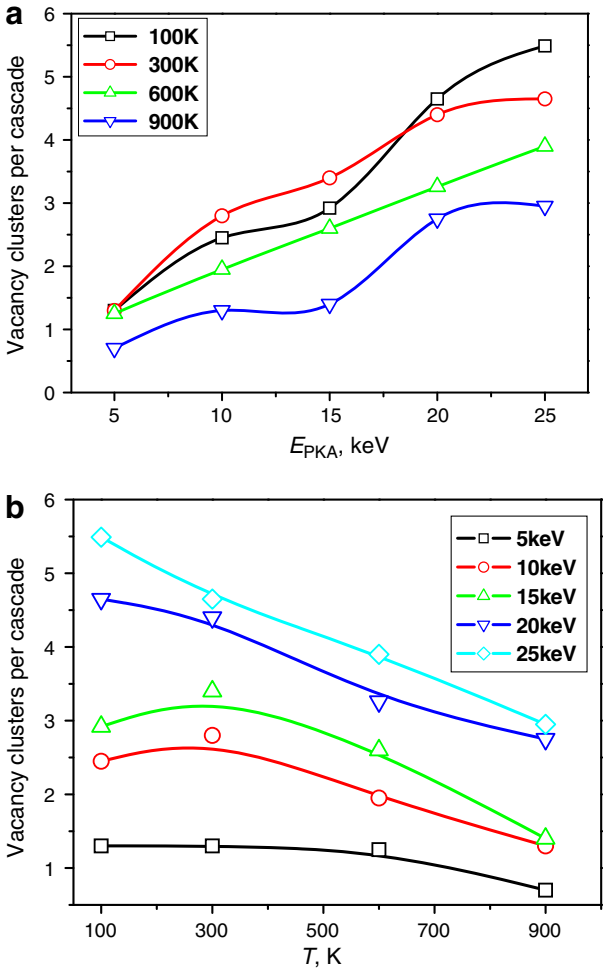


**Fig. 9.** Variation of the mean number of vacancy clusters (of size three or more) created per cascade versus (a) cascade energy and (b) irradiation temperature.

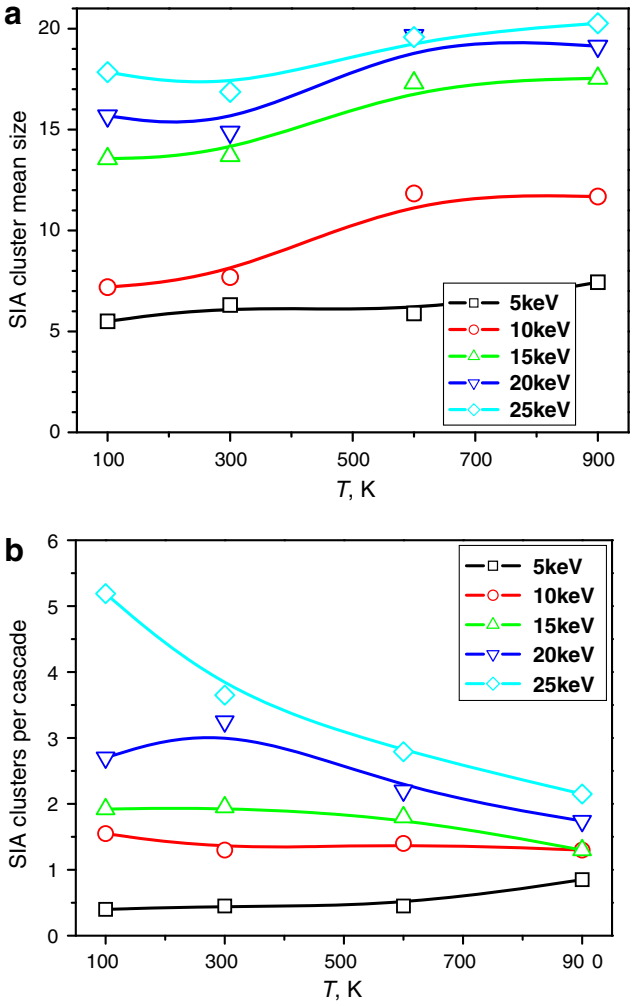


**Fig. 10.** (a) Variation with $T$ of the mean number of SIAs per interstitial cluster of size four or more. (b) Variation with $T$ of the mean number of interstitial clusters (of size four or more) created per cascade.

increases the probability of interstitial-vacancy recombination, resulting in reduction in $N_{FP}$, but also reduces the stability of vacancy clusters. Although the cluster mean size of both species is similar at low $T$, SIA clusters are formed with larger mean size at high $T$, probably reflecting the greater stability (higher binding energy) of these defects.

The trends in the plots of yield of vacancy and interstitial clusters in Figs. 9(b) and 10(b) are qualitatively and quantitatively similar. This suggests a correlation in the formation of the two cluster types in individual cascades. Correlations in spatial distribution and size of extended clusters constitute a topic to be addressed in detail in part II [26].

## 7. Discussion and conclusions

The results reported here are the outcome of the largest set of simulations of displacement cascades in copper to date. They span ranges of energy and temperature of interest for basic research into the performance of FCC metals in an irradiation environment. The defect number and configuration vary strongly from cascade to cascade, and so we have attempted to generate and analyse a sufficient number of cascades for each condition of $E_{PKA}$ and $T$ to determine data and detect trends with statistical significance. Computational techniques described in Section 2 have been

adopted to increase the model size usable for a given cascade energy and to enhance the efficiency of data analysis.

The number of point defects and the statistics of their clustering are the main concerns of this paper. Generally, the number of vacancies or SIAs per cascade is only 15–20% of the NRT predicted value. This fraction is reduced to the lower end of the range by increasing temperature, particularly for cascade energy above 10–15 keV. This is reflected in the decrease of the exponent m from 1.15 to 1.05 in the best-fit line $N_{FP} = A(E_{PKA})^m$ through the mean data between 100 and 900 K (Fig. 3). The biggest effect of increasing $T$ in this energy range occurs between 600 and 900 K. The explanation for this lies in the influence of high temperature for reducing effective cascade volume and increasing lifetime of the thermal spike. Both effects enhance defect recombination. Note, however, that these trends are for the mean values: individual cascades can show considerable variations from the mean. For example, $N_{FP}$ for the 52 cascades simulated with $E_{PKA} = 25$ keV and $T = 100$ K has a mean of 69, but the individual values range from 23 to 122 (see Fig. 2). This emphasises the importance of capturing information from as many cascades as possible. Four or five, as in the early days of cascade simulation by MD, are insufficient.

It has been conventional practice in this field to analyse the statistics of point defect clustering during the cascade process, i.e. by the end of the thermal spike phase, by defining a clustered defect as one with at least one neighbour of the same type in a near-neighbour position. (The appropriate position is first-nearest neighbours for FCC metals because the binding energy of divacancies and di-interstitials is highest in this arrangement.) The data for the clustered fractions $\varepsilon_2^v$ and $\varepsilon_2^i$ in Fig. 4 are based on this and, despite the wide dispersion in the fraction for individual cascades, both show a clear increasing trend with increasing $E_{PKA}$. The main features are (a) $\varepsilon_2^i$ is significantly higher than $\varepsilon_2^v$, rising to 70–90% at 25 keV, irrespective of $T$, and (b) although $\varepsilon_2^v$ does not vary significantly with $T$ in the range $\leqslant 600$ K, it is decreased substantially (to about 20%) at 900 K. These variations can be explained in qualitative terms by a combination of the influence of $T$ on cascade volume and lifetime discussed above, and the lower stability (lower binding energy) of vacancy clusters compared with SIA clusters.

In addition to studying the numbers of defects, we have attempted to categorise the defect clusters that typically arise in cascades in copper. They are illustrated by the visualised configurations in Fig. 6. The clustered SIAs tend to form either perfect ($\boldsymbol{b} = 1/2\langle 1\,1\,0\rangle$) or faulted ($\boldsymbol{b} = 1/3\langle 1\,1\,1\rangle$) dislocation loops. Large, 3-D clusters can arise, but they are unstable with respect to the perfect arrangement during sufficient post-cascade annealing. These dislocation defects are either mobile in one direction ($\boldsymbol{b}$) if perfect or sessile if either faulted or untransformed, and have size of four interstitials or more. It can be seen from Fig. 7(b) for $\varepsilon_4^i$ (and by comparing with Fig. 5(d) for $\varepsilon_2^i$) that the majority of SIAs are in this form for $E_{PKA} \geqslant 15$ keV. Importantly, this result holds irrespective of irradiation temperature.

The clustered vacancies, in contrast, almost inevitably form 3-D configurations with {1 1 1} faces. In a few cases, these are almost regular SFTs (Fig. 6(a)); in most they are conjoined SFTs (Fig. 6(b)) or even more irregular polyhedra (Fig. 6(c)). The <1 1 0> edges of these extended defects are stair-rod partial dislocations and so their strain field is short-ranged compared with that of the SIA loops. Tetrahedral clusters become stable for size of three or more vacancies. Fig. 7(a) for $\varepsilon_3^v$ shows that about 40% of the vacancy population have SFT-like character on the average for cascades with $E_{PKA} \geqslant 15$ keV when $T \leqslant 600$ K. The proportion falls to 10–20% at 900 K, however, emphasising once again the significant influence the irradiation temperature has on the vacancy component of the primary state of cascade damage. The size spectrum of the SFT-like clusters created in the simulations can be compared directly with size data found in recent experiments on neutron-irradiated copper [24]. This leads to the conclusion that the SFTs observed in experiment are formed directly in the core of cascades as part of the primary damage state, as discussed further in part II [26].

Finally, it was noted in Section 6.2 that the trends in the plots of yield per cascade of vacancy and interstitial clusters (Figs. 9(b) and 10(b)) are similar, thereby suggesting a correlation in the formation of the two cluster types in individual cascades. This is also apparent from the computer-generated visualisations we have carried out: Figs. 5(b) and 6(d) and (f) are just a few examples. It seems that the creation of one cluster aids that of the other type. Furthermore, the visualisations suggest that they form close together, without annihilation. These issues have been quantified and the resulting correlations in spatial distribution and size of extended defect clusters are described in detail in part II. The stability of SFTs and loops, and the proximity of clusters of different nature have an influence on defect production when one cascade overlaps the debris of another. This affects defect production efficiency at high irradiation dose. This aspect is also considered in part II.

## Acknowledgements

This research was supported by a research Grant EP/D047684/1 ('Alloys By Design – A Materials Modelling Approach') from the UK Engineering and Physical Sciences Research Council, by grant F1R1-CT-2001-20136 ('ITEM') from the Council of the European Commission and by the Division of Materials Sciences and Engineering and the Office of Fusion Energy Sciences, US. Department of Energy, under contract DE-AC05-00OR22725 with UT-Battelle, LLC.

## References

[1] D.J. Bacon, T. Diaz de la Rubia, J. Nucl. Mater. 216 (1994) 275.
[2] D.J. Bacon, A.F. Calder, F. Gao, V.G. Kapinos, S.J. Wooding, Nucl. Instrum. and Meth. B 102 (1995) 37.
[3] D.J. Bacon, A.F. Calder, F. Gao, J. Nucl. Mater. 251 (1997) 1.
[4] D.J. Bacon, F. Gao, Yu.N. Osetsky, J. Nucl. Mater. 276 (2000) 1.
[5] D.J. Bacon, Yu.N. Osetsky, R. Stoller, R.E. Voskoboinikov, J. Nucl. Mater. 323 (2003) 152.
[6] T. Diaz de la Rubia, R.S. Averback, H. Hsieh, R. Benedek, J. Mater. Res. 4 (1989) 579.
[7] T. Diaz de la Rubia, M.W. Guinan, Mater. Res. Forum. 97–99 (1992) 23.
[8] T. Diaz de la Rubia, W.J. Phythian, J. Nucl. Mater. 191–194 (1992) 108.
[9] T. Diaz de la Rubia, M.W. Guinan, A. Caro, Radiat. Eff. Def. 130&131 (1994) 39.
[10] A.J.E. Foreman, W.J. Phythian, C.A. English, J. Nucl. Mater. 129 (1994) 25.
[11] W.J. Phythian, R.E. Stoller, A.J.E. Foreman, A.F. Calder, D.J. Bacon, J. Nucl. Mater. 223 (1995) 245.
[12] K. Nordlund, R.S. Averback, Phys. Rev. B 56 (1997) 2421.
[13] Yu.N. Osetsky, D.J. Bacon, Nucl. Instrum. and Meth. B 180 (2001) 85.
[14] Yu.N. Osetsky, D.J. Bacon, B.N. Singh, J. Nucl. Mater. 307 (2002) 866.
[15] R.E. Voskoboinikov, Yu.N. Osetsky, D.J. Bacon, J. ASTM Int. 2 (8) (2005).
[16] M. Kiritani, T. Yoshie, S. Kojima, J. Nucl. Mater. 141–143 (1986) 625.
[17] A. Calder, D.J. Bacon, W.J. Phythian, C.A. English, Mater. Sci. Forum. 97–99 (1992) 183.
[18] T.L. Daulton, M.A. Kirk, L.E. Rehn, Philos. Mag. A 80 (2000) 809.
[19] C.C. Matthai, D.J. Bacon, J. Nucl. Mater. 135 (1985) 173.
[20] V.G. Kapinos, Yu.N. Osetsky, P.A. Platonov, Soviet. Phys. Solid State 28 (1986) 3603.
[21] V.G. Kapinos, Yu.N. Osetsky, P.A. Platonov, J. Nucl. Mater. 165 (1989) 286.
[22] Yu.N. Osetsky, M. Victoria, A. Serra, V. Priego, S.I. Golubov, J. Nucl. Mater. 251 (1997) 34.
[23] B.N. Singh, M. Eldrup, A. Horsewell, P. Ehrhart, F. Dworschak, Philos. Mag. A 80 (2000) 2628.
[24] B.N. Singh, D.J. Edwards, P. Toft, J. Nucl. Mater. 299 (2001) 205.
[25] Yu.N. Osetsky, D.J. Bacon, B.N. Singh, J. Nucl. Mater. 307–311 (2002) 866.
[26] R.E. Voskoboinikov, Yu.N. Osetsky, D.J. Bacon, submitted for publication.
[27] G.J. Ackland, G. Tichy, V. Vitek, M.W. Finnis, Philos. Mag. A 56 (1987) 735.
[28] V.G. Kapinos, D.J. Bacon, Phys. Rev. B 50 (1994) 13194.
[29] Yu.N. Osetsky, D.J. Bacon, Z. Rong, B.N. Singh, Philos. Mag. Lett. 84 (2004) 745.
[30] Y. Mishin, M.J. Mehl, D.A. Papaconstantopoulos, A.F. Voter, J.D. Kress, Phys. Rev. B 63 (2001) 224106.

[31] J.P. Biersack, J.F. Ziegler, Nucl. Instrum. and Meth. 194 (1982) 93.
[32] W.L. Wood, Practical Time-stepping Schemes, Clarendon, Oxford, 1990.
[33] D. Frenkel, B. Smit, Understanding molecular simulation, From Algorithms to Applications, Academic Press, 1996.
[34] M.J. Norgett, M.T. Robinson, I.M. Torrens, Nucl. Eng. Design 33 (1975) 50.
[35] Standard E521, ASTM Annual Book of Standards (1989).
[36] R.E. Stoller, J. Nucl. Mater. 276 (2000) 22.
[37] Yu.N. Osetsky, D.J. Bacon, A. Serra, B.N. Singh, S.I. Golubov, Philos. Mag. 83 (2003) 61.
[38] B.N. Singh, S.I. Golubov, H. Trinkhaus, A. Serra, Yu.N. Osetsky, A.V. Barashev, J. Nucl. Mater. 251 (1997) 107.